



1 **Modelled estimates of spatial variability of iron stress in the**
2 **Atlantic sector of the Southern Ocean**

3

4 Thomas J. Ryan-Keogh^{1,2}, Sandy J. Thomalla¹, Thato N. Mtshali¹, Hazel Little²

5

6 ¹Southern Ocean Carbon and Climate Observatory, Natural Resources and Environment, CSIR, Rosebank, Cape
7 Town 7700, South Africa

8 ²Department of Oceanography, University of Cape Town, Rondebosch, Cape Town 7701, South Africa

9

10 *Correspondence to:* Thomas.Ryan-Keogh@uct.ac.za

11

12 **Abstract**

13

14 The Atlantic sector of the Southern Ocean is characterized by markedly different frontal zones with specific
15 seasonal and sub-seasonal dynamics. Demonstrated here is the effect of iron on the potential maximum
16 productivity rates of the phytoplankton community. A series of iron addition productivity versus irradiance (PE)
17 experiments utilising a unique experimental design that allowed for 24 hour incubations were performed within
18 the austral summer of 2015/16. The addition of iron can result in the doubling of the photosynthetic parameters
19 α^B and P^B_{max} , with subsequent changes in E_k . Mean values for each parameter under iron replete conditions were
20 1.46 ± 0.55 ($\mu\text{g} (\mu\text{g Chl a})^{-1} \text{h}^{-1}$ ($\mu\text{M photons m}^{-2} \text{s}^{-1}$)⁻¹), 72.55 ± 27.97 ($\mu\text{g} (\mu\text{g Chl a})^{-1} \text{h}^{-1}$) and 50.84 ± 11.89 (μM
21 $\text{photons m}^{-2} \text{s}^{-1}$); whereas mean values under the control conditions were 1.25 ± 0.92 ($\mu\text{g} (\mu\text{g Chl a})^{-1} \text{h}^{-1}$ (μM
22 $\text{photons m}^{-2} \text{s}^{-1}$)⁻¹), 62.44 ± 36.96 ($\mu\text{g} (\mu\text{g Chl a})^{-1} \text{h}^{-1}$) and 55.81 ± 19.60 ($\mu\text{M photons m}^{-2} \text{s}^{-1}$). There were no clear
23 spatial patterns in either the absolute values or the absolute differences between the treatments at the
24 experimental locations. When these parameters are integrated into a standard depth-integrated primary
25 production model across a latitudinal transect, the effect of iron addition shows higher levels of primary
26 production south of 50°S, with very little difference observed in the sub-Antarctic and Polar Frontal zone. These
27 results emphasize the need for better parameterisation of photosynthetic parameters in biogeochemical models
28 around sensitivities in their response to iron supply. Future biogeochemical models will need to consider the
29 combined and individual effects of iron and light to better resolve the natural background in primary production
30 and predict its response under a changing climate.

31



32 1. Introduction

33

34 Phytoplankton primary production (PP) in the Southern Ocean is a key contributor to global atmospheric CO₂
35 drawdown, responsible for 30-40% of global anthropogenic carbon uptake (Khatiwala et al., 2009; Mikaloff
36 Fletcher et al., 2006; Schlitzer, 2002). High nutrient availability fuels this phytoplankton production, but growth
37 is ultimately constrained by the lack of availability of the micronutrient iron (Fe) (de Baar et al., 1990; Martin et
38 al., 1990). This leads to high levels of macronutrients that remain unutilised by phytoplankton growth in what is
39 known as a High Nutrient Low Chlorophyll (HNLC) conditions. Maximum primary productivity rates of the
40 Southern Ocean are also limited by light availability due to low incident solar angles, persistent cloud cover and
41 deep mixed layers that curtail production and subsequently affect the efficiency of the biological carbon pump.
42 Under future climate change scenarios, altered upwelling and mixed layer stratification (Boyd et al., 2001; Boyd
43 and Doney, 2002), changes in sea ice cover (Arrigo et al., 2013; Montes-Hugo et al., 2008) and food-web
44 dynamics (Dubischar and Bathmann, 1997; Moore et al., 2013; Pakhomov and Froneman, 2004; Smetacek et
45 al., 2004) will alter both the nutrient and light supply strongly impacting primary production rates. As such, it is
46 important that we understand the sensitivity of phytoplankton production to light and micronutrient availability
47 so that we may improve our predictive capability of the response of the Southern Ocean carbon pump to a
48 changing climate.

49 Iron plays a critical role in modulating PP due to the high requirements of the photosynthetic apparatus,
50 photosystems I and II (Raven, 1990; Shi et al., 2007; Strzepek and Harrison, 2004). Light availability can
51 further increase the demand for iron, as low irradiance levels increase requirements associated with the synthesis
52 of additional photosynthetic units to increase potential light absorption (Maldonado et al., 1999; Raven, 1990;
53 Strzepek et al., 2012; Sunda and Huntsman, 1997). Iron is also required to activate both nitrate and nitrite
54 reductase (de Baar et al., 2005), which facilitate the assimilation of nitrate and nitrite and their subsequent
55 intracellular reduction to ammonium. In HNLC regions, such as the Southern Ocean, nitrate uptake rates (ρNO_3^-
56) have also frequently been reported as becoming iron limited (Cochlan, 2008; Lucas et al., 2007; Moore et al.,
57 2013; Price et al., 1994). However, it has also been demonstrated that iron limitation rather than inhibiting
58 nitrate reductase activity results in a bottleneck further downstream due to a reduction in photosynthetically
59 derived reductant (Milligan and Harrison, 2000). This would lead to an excretion of excess nitrate back into the
60 water column that would further contribute to HNLC conditions such as those present in the Southern Ocean.

61 Estimating PP in the oceans towards an improved understanding of the effects of iron and light
62 limitation requires an understanding of the relationship between photosynthesis (P) and irradiance (E)
63 (Behrenfeld and Falkowski, 1997b; Dower and Lucas, 1993; Platt et al., 2007). PE responses are derived from
64 an equation by Platt et al. (1980), where the responses are parameterized as a function of irradiance. The
65 parameters derived include: P_{max}^B , the biomass-specific rate of photosynthesis at saturating irradiances, α^B , the
66 irradiance-limited biomass-specific initial slope, and E_k , the irradiance at which saturation is initiated. The
67 response of these parameters can be a function of temperature (Behrenfeld and Falkowski, 1997b), but also as a
68 change in the quantum efficiency of photosynthesis, usually as the result of changes in iron availability. In
69 previous iron fertilization experiments a doubling of α^B has been reported (Hiscock et al., 2008), yet this
70 response is not consistent across Southern Ocean waters (Feng et al., 2010; Hopkinson et al., 2007; Moore et al.,
71 2007; Smith and Donaldson, 2015). Given their relative importance within PP models (Behrenfeld and



72 Falkowski, 1997a, b; Sathyendranath and Platt, 2007), a greater understanding of the drivers of the variability
73 within these photosynthetic parameters is therefore required; particularly if we are to accurately quantify and
74 constrain PP in the Southern Ocean to examine seasonal and interannual variability and trends.

75 The Atlantic sector of the Southern Ocean is composed of a series of circumpolar fronts that are
76 characterized by large geostrophic velocities (Nowlin and Klinck, 1986; Orsi et al., 1995). The fronts constrain
77 water masses with distinct physical and chemical properties that define different oceanographic zones. These
78 spatial zones, whilst not only displaying zonal variability with the fronts, also display important seasonal
79 contrasts (Thomalla et al., 2011), with differing bloom initiation dates and temporal extent of bloom duration.
80 Whilst the bloom initiation dates can in part be explained by day length and sea ice cover as you move
81 polewards, the differences in the extent and duration of blooms between the zones requires an alternative and
82 more nuanced explanation. One theory that has been postulated is that the supply mechanisms of iron to the
83 mixed layer following the spring bloom varies between zones (Thomalla et al., 2011). Weak diapycnal inputs
84 and a heavy reliance on iron recycling was suggested by Tagliabue et al. (2014) to match approximate
85 phytoplankton utilization within the pelagic zones. An alternative theory that postulates the importance of
86 summer storms may also be pivotal in understanding the seasonal dynamics of phytoplankton primary
87 productivity (Nicholson et al., 2016; Swart et al., 2015; Thomalla et al., 2015), with respect to the sustained
88 bloom observed in the Sub Antarctic Zone (SAZ). Here, summer storms are said to periodically deepen the
89 mixed layer to below the ferricline followed by rapid shoaling during quiescent periods that balances the supply
90 of light and iron in the upper oceans favouring phytoplankton growth that culminates in a sustained summer
91 bloom (Swart et al., 2015). Regardless of the mechanisms at play, an understanding on when and where iron
92 concentrations and supply mechanisms limits potential phytoplankton growth and productivity is needed to
93 better understand the drivers that determine the characteristics of the Southern Ocean seasonal cycle.

94 To this end, a research cruise was conducted in the austral summer of 2015/16 as part of the third
95 multidisciplinary *Southern Ocean Seasonal Cycle Experiment* (SOSCEX III) which aims to identify and
96 understand the physical and chemical controls on the seasonal cycle of the biological carbon pump. As part of
97 this study, shipboard nutrient addition PE experiments were performed to determine the extent of iron limitation
98 upon phytoplankton primary production.

99



100 2. Materials and Methods

101

102 2.1. Oceanographic Sampling

103

104 The samples and data presented here were obtained during the 55th South African National Antarctic Expedition
105 (3rd December 2015 to 11th February 2016) on-board the S.A. Agulhas II to the Atlantic sector of the Southern
106 Ocean as part of SOSCEX III (Swart et al., 2012). During the cruise, 6 nutrient addition PE long-term
107 experiments were performed within the Atlantic sector of the Southern Ocean (Fig. 1) to determine the extent to
108 which relief from iron limitation could alter the maximal primary productivity rates of the phytoplankton
109 community. Uncontaminated whole seawater was collected from 30-50 m depth using Teflon-lined, external
110 closure 12 L Go-Flo samplers deployed on a trace metal clean CTD rosette system.

111

112 2.2. PE Experimental setup

113

114 Phytoplankton productivity was measured by the incorporation of ¹³C stable isotopes in response to an
115 increasing light gradient. Inside a trace metal clean laboratory container, bulk trace metal clean seawater was
116 decanted unscreened into an acid-washed 50 L LDPE carboy (Thermo scientific) to ensure homogenization; this
117 was then redistributed into 1.0 L polycarbonate bottles (Nalgene). Sample manipulations were conducted under
118 a laminar flow hood. All bottles were inoculated with ¹³C (10 μM NaH₂¹³CO₃/ 100 mL) spikes to achieve an
119 enrichment of ~5%; 11 bottles received the addition of FeCl₃ (+2.0 nM, 'Fe'), whereas 11 bottles received the
120 ¹³C spikes alone ('Control'). The bottles were incubated in screened (LEE Filters) LDPE boxes within light and
121 temperature controlled incubators. Experimental temperature was set to mimic the *in situ* sample collection
122 temperature. Irradiances were measured within the screened boxes using a handheld 4π PAR sensor
123 (Biospherical Instruments) and ranged from 0 – 400 μM photons m⁻² s⁻¹. Bottles tops were covered with
124 parafilm and double bagged with clear polyethylene bags to minimize contamination risks during the
125 incubation.

126 Experiments were incubated for 24 h, after which the samples were vacuum filtered through a pre-
127 combusted (400°C for 24 h) GF/F filter. Samples were acid fumed with concentrated HCl for 24 h to remove
128 inorganic carbon before being dried in an oven at 40°C for 24 h. The isotopic composition of all samples were
129 determined by mass spectrometry on a Flash EA 1112 series elemental analyser (Thermo Finnigan). Carbon
130 uptake rates (μM C h⁻¹) were calculated from the equation of Dugdale and Wilkerson (1986), utilising *in situ*
131 determinations of dissolved inorganic carbon (DIC). The uptake rates normalised to the chlorophyll-a (Chl)
132 concentration, were used to calculate the maximal light-saturated Chl specific photosynthetic fixation rates
133 (P_{max}^B), the light limited slope (α^B) and the photoacclimation parameter (E_k). The curves and parameters were
134 generated using a non-linear least squares fit to the equation of Platt et al. (1980).

135

136



137 Table 1 Locations for PE experiments conducted during the cruise along with details for the initial chemical,
 138 physiological and physical set up conditions.

Experiment	1	2	3	4	5	6
Initiation Date	08/12/2015	05/01/2016	07/01/2016	08/01/2016	09/01/2016	26/01/2016
Latitude (°S)	-42.69	-42.69	-45.99	-50.45	-55.70	-70.44
Longitude (°E/W)	08.74	08.74	05.93	01.04	-00.00	-07.82
Collection Depth (m)	30	35	35	35	50	35
Sunrise:	03:30	04:00	04:00	04:00	04:00	00:00
Sunset	18:30	19:00	19:00	19:00	19:00	00:00*
Chl ($\mu\text{g L}^{-1}$)	0.97	0.84	0.89	2.30	1.15	1.49
Nitrate (μM)	7.21	10.20	15.83	21.07	17.02	23.81
Silicate (μM)	0.86	0.72	0.09	3.76	30.83	48.81
Phosphate (μM)	0.88	0.76	0.95	1.28	1.11	0.94
DFe (nM)	0.16	0.17	0.07	0.03	0.05	0.10
F_v/F_m	0.19	0.30	0.35	0.30	0.35	0.37
σ_{PSII} (nm^{-2})	14.79	6.45	5.50	5.59	5.37	3.89
MLD (m)	33.77	56.96	108.42	70.11	42.89	40.80
Salinity	33.87	33.70	33.88	33.80	36.51	34.10
Temp. (°C)	10.80	10.44	6.72	3.17	-1.42	-1.51
Average daytime PAR ($\mu\text{M photons m}^{-2} \text{s}^{-1}$)**	1055.31	787.35	289.18	524.41	769.87	673.62
Euphotic Depth (m)	72.79	75.10	52.95	47.92	69.13	78.07

139 *24 hour day length

140 **See Sect. 2.7 for details

141

142 2.3. Chlorophyll-a and Nutrient Analysis

143



144 Samples for Chl analysis, 250 mL, were filtered onto GF/F filters and then extracted into 90% acetone for 24 h
145 in the dark at -20°C, followed by analysis with a fluorometer (TD70; Turner Designs) (Welschmeyer, 1994).
146 Macronutrient samples were drawn into 50 mL diluivials and stored at -20°C until analysis on land. Nitrate +
147 Nitrite and Silicate were measured using a Lachat Flow Injection Analyser (Egan, 2008; Wolters, 2002), whilst
148 Nitrite and Phosphate were determined manually by colorimetric method as specified by Grasshoff et al. (1983).
149 Dissolved iron samples (DFe) were carefully collected in acid-washed 125 mL LDPE bottles, acidified with
150 30% HCl suprapur to pH ~1.7 (using 2 mL L⁻¹ criteria) and stored at room temperature until analysis on land at
151 UniBrest in France using the Chemiluminescence – Flow Injection Analyser (CL-FIA) method (Obata et al.,
152 1993). Accuracy and precision of the method was verified by analysis of in-house internal standards and SAFe
153 reference seawater samples (Johnson et al., 2007); the limits of detection were in order of 10 pM.

154

155 **2.4. Phytoplankton Photosynthetic Physiology**

156

157 Variable Chl fluorescence was measured using a Chelsea Scientific Instruments FastOcean fast repetition rate
158 fluorometer (FRRf) integrated with a FastAct laboratory system. Samples were acclimated in dark bottles at *in*
159 *situ* temperatures, and FRRf measurements were blank corrected using carefully prepared 0.2 µm filtrates for all
160 samples (Cullen and Davis, 2003). Protocols for FRRf measurements consisted of the following: 100 x 2 µs
161 saturation flashlets with a 2 µs interval, followed by 25 x 1 µs relaxation flashlets with an interval of 84 µs with
162 a sequence interval of 100 ms. Sequences were repeated 32 times resulting in an acquisition length of 3.2 s. The
163 power of the excitation LED (λ450), was adjusted between samples to saturate the observed fluorescence
164 transients within a given range of $R\sigma_{PSII}$. $R\sigma_{PSII}$, the probability of a reaction centre being closed during the first
165 flashlet, is optimised between 0.042 to 0.064 per the manufacturer specifications. By adopting this approach, it
166 ensures the best signal-to-noise ratio in the recovered parameters whilst accommodating significant variations in
167 the photophysiology of the phytoplankton community without having to adjust the protocol. Data from the
168 FRRf were analysed to derive fluorescence parameters as defined in Baker et al. (2001) and Roháček (2002) by
169 fitting transients to the model of Kolber et al. (1998).

170

171 **2.5. Pigment Analysis and CHEMTAX**

172

173 Pigment samples were collected by filtering 0.5 – 2.0 L of water onto GF/F filters. Filters were frozen and
174 stored at -80°C until analysis in Villefranche, France on a HPLC Agilent Technologies 1200. Filters were
175 extracted in 100% methanol, disrupted by sonication, clarified by filtration and analysed by HPLC following the
176 methods of Ras et al. (2008). Limits of detection were on the order of 0.1 ng L⁻¹. Pigment composition data were
177 standardized through root square transformation before cluster analysis utilizing multi-dimensional scaling
178 where similar samples appear together; and dissimilar samples do not. Samples were grouped and analysed in
179 CHEMTAX (Mackey et al., 1996) using the pigment ratios from Gibberd et al. (2013). Multiple iterations of
180 pigment ratios were used to reduce uncertainty in the taxonomic abundance as described in Gibberd et al.
181 (2013), with the solution that had the smallest residual used for the estimated taxonomic abundance.

182

183 **2.6. Particle Size Analysis**



184

185 The size distribution of the particle population was measured by running 40 mL of water sample through a 100
 186 μm aperture on a Beckman Coulter-Multisizer (20 runs at 2.0 mL per run), binning the size counts into 400 bins
 187 between 2 μm and 60 μm . Data were subsequently analysed utilising custom Matlab scripts to calculate the
 188 effective diameter of particles within the sample following Hansen and Travis (1974).

189

190 2.7. Depth-integrated Production

191

192 Water column primary production rates were calculated according to Platt et al. (1980) and Platt and
 193 Sathyendranath (1993) as in Thomalla et al. (2015) where;

194

$$195 \quad PP_0 = P_{max} \times \left(1 - e^{\frac{-\alpha \times E_0^m \times 0.5}{P_{max}}}\right) \quad (1)$$

196

197 PP_0 ($\text{mg C m}^{-2} \text{ d}^{-1}$) is the primary production at the surface, P_{max} the maximal light-saturated photosynthetic
 198 fixation rate, α the light-limited slope and E_0^m is daily PAR at the surface, calculated by assuming maximum
 199 PAR at midday, zero PAR at sunrise and sunset, a constant gradient of light between time steps and
 200 extrapolating the measured PAR (from an above water Biospherical 4π PAR sensor) at the time of the station
 201 into an isosceles triangle (see also Thomalla et al. (2015)).

202

$$203 \quad E_*^m = \frac{E_0^m}{E_k} \quad (2)$$

204

205 The results were generalised by calculating $E_*^m(2)$, the dimensionless daily surface irradiance, while primary
 206 productivity over the entire water column PP_{wc} ($\text{mg C m}^{-2} \text{ d}^{-1}$) was calculated with the following equation (3).
 207 The dimensionless function $f(E_*^m)$ for daily primary productivity was solved analytically by Platt et al. (1980).
 208 Rates were calculated for both the iron addition and control treatments, allowing the difference between the
 209 integrated rates to be solved.

210

$$211 \quad PP_{wc} = PP_0 \times \frac{f(E_*^m)}{k_d} \quad (3)$$

212

213 K_d was initially calculated as the slope of the natural log of in situ PAR with depth from CTD profiles. When in
 214 situ PAR with depth was not available, K_d was also calculated from *in situ* surface Chl concentrations with the
 215 following equation (4) (Morel, 1988; Morel et al., 2007). Co-located calculations utilising in situ PAR versus
 216 chlorophyll-derived K_d demonstrated on average a 40% higher K_d when calculated with chlorophyll.

217

$$218 \quad K_d = 0.0166 + 0.0773 \times [Chl]^{0.6715} \quad (4)$$

219

220 2.8. Ancillary physical data

221



222 Temperature and salinity profiles were obtained from a Sea-Bird CTD mounted on the rosette system. The
223 mixed layer depth (MLD) was calculated following de Boyer Montégut et al. (2004), which identifies the MLD
224 as the depth where the temperature differs from the temperature at 10 m by more than 0.2°C ($\Delta T_{10\text{m}} = 0.2^{\circ}\text{C}$).
225 The position of the fronts was determined using sea surface height (SSH) data from maps of absolute dynamic
226 topography (MADT) according to (Swart et al., 2010).



227 3. Results

228

229 3.1. Oceanographic Context

230

231 The experimental set-up locations covered a wide range of pelagic zones from the SAZ to the Marginal Ice Zone
232 (MIZ), each with different physical, chemical and biological properties (see Table 1). Chl concentrations
233 between experiment initiation locations varied between $0.84 - 2.30 \mu\text{g L}^{-1}$, peaking just south of the Polar Front
234 at $\sim 50^\circ\text{S}$. Initial temperatures displayed a characteristic decrease from 10.80°C at the most northerly location to
235 -1.51°C at the MIZ, whereas there were no distinct differences in salinity ranging from 33.71 to 36.51.
236 Macronutrient concentrations all increased polewards, with peaks of $28.15 \mu\text{M}$, $1.34 \mu\text{M}$ and $48.81 \mu\text{M}$ for
237 nitrate, phosphate and silicate respectively. Dissolved iron concentrations decreased polewards from a
238 maximum of 0.17 nM in the SAZ to minimum values of 0.03 nM and 0.05 nM at 50°S and 55°S respectively,
239 before increasing again in the MIZ to 0.10 nM .

240 Phytoplankton photophysiology, F_v/F_m , increased polewards from a minimum of 0.19 to a maximum of
241 0.37, whereas σ_{PSII} , the effective absorption cross-section of PSII, decreased polewards from 14.79 nm^{-2} to 3.89
242 nm^{-2} . The effective diameter of the phytoplankton population, a relative measure of size, increased polewards
243 from a minimum of $4.29 \pm 0.35 \mu\text{m}$ in the SAZ to a maximum of $8.59 \pm 0.68 \mu\text{m}$ in the MIZ. Estimated taxonomic
244 abundance through HPLC analysis and CHEMTAX determined that the dominant groups at all stations were
245 either Diatoms, Haptophytes or a mix of the two. Haptophytes were the dominant group ($>68\%$ of total Chl) in
246 the SAZ during experiments 1 and 2, with Diatoms becoming dominant ($>70\%$ of total Chl) from experiment 4
247 onwards.

248 MLD's were highly variable and ranged from $\sim 34\text{m}$ at experiment 1 to $\sim 108 \text{ m}$ at experiment 3. The
249 MLD was typically deeper than the experimental set up depth (average difference of $\sim 15 \text{ m}$) at all experiments
250 except for experiment 5 where the collection depth was 7 m below the MLD. Experiments 1 and 2 that were set
251 up in the same location in the SAZ but 28 days apart had markedly different set up conditions; a 41% increase in
252 the nitrate concentration from 7.21 to $10.20 \mu\text{M}$, a two-fold increase in F_v/F_m from 0.19 to 0.35 with a
253 concurrent 56% decrease in σ_{PSII} from 14.79 to 6.45 nm^{-2} and a deepening of the MLD from $\sim 34 \text{ m}$ to $\sim 57 \text{ m}$.

254 The light environment within the water column at each location was determined by calculating the
255 percentage light depth as a function of the vertical attenuation coefficient of irradiance (K_d). The percentage
256 light depths of the experiments ranged between 3.46% to 14.78%. The 1% light depth, which typically coincides
257 with the compensation light depth i.e. the depth where rates of production equate to rates of respiration, is
258 consistently below the MLD, except for experiment 4 where it was 22 m above the mixed layer.

259

260 3.2. PE Parameters

261

262 PE curves for carbon uptake (ρC) (Fig. 2, Fig. S1), summarised in Table 2, display consistent results with
263 greater values of α^{B} and $P^{\text{B}}_{\text{max}}$ with the addition of iron compared to the control treatments (Fig. S2). The values
264 derived here fall within the range previously reported for iron addition experiments in the Southern Ocean
265 (Hiscock et al., 2008; Hopkinson et al., 2007; Moore et al., 2007; Smith and Donaldson, 2015). Maximum
266 values of α^{B} ($\text{mg C (mg Chl a)}^{-1} \text{ h}^{-1}$ ($\mu\text{mol photons m}^{-2} \text{ s}^{-1}$) $^{-1}$) for ρC were 2.23×10^{-3} from experiment 2 Fe



267 treatment and 2.43×10^{-3} from experiment 1 control treatment, with minimum values of 0.13×10^{-3} from
 268 experiment 5 control treatment and 0.56×10^{-3} from experiment 6 Fe treatment. P_{\max}^B ($\text{mg C} (\text{mg Chl a})^{-1} \text{h}^{-1}$)
 269 values peaked in experiment 1 Fe treatment, with a minimum value of 1.06×10^{-2} in experiment 5 control
 270 treatment. E_k ($\mu\text{mol photons m}^{-2} \text{s}^{-1}$) peaked at 79.77, with minimum values in experiment 1 control treatment.
 271 Despite the substantial differences in set up conditions for experiments 1 and 2 in the SAZ, occupied twice over
 272 the space of 28 days, there were no significant differences in the responses of the PE parameters to Fe.

273 To better understand the effects of iron limitation on the PE parameters, the absolute differences (Fig.
 274 3) of α^B , P_{\max}^B , and E_k between the iron treatments and control treatments were calculated. $\Delta\alpha^B$ ranged from -
 275 6.94×10^{-4} to 1.30×10^{-3} , with minimum and maximum percentage differences of -40.04% and 91.12%
 276 respectively. ΔP_{\max}^B ranged between 4.98×10^{-2} and -1.02×10^{-2} , with minimum and maximum percentage
 277 differences of -12.10% and 82.52%; the greatest value for ΔE_k was -40.92 for experiment 5. Maximal values of
 278 all differences were consistently found in experiment 5 which was set up just south of the Southern Boundary
 279 front (Figure 3).

280

281 Table 2 Summary of PE parameters, α^B ($\text{mg} (\text{mg Chl a})^{-1} \text{h}^{-1}$ ($\mu\text{mol photons m}^{-2} \text{s}^{-1}$)⁻¹), P_{\max}^B ($\text{mg} (\text{mg Chl a})^{-1} \text{h}^{-1}$)
 282 ¹) and E_k ($\mu\text{mol photons m}^{-2} \text{s}^{-1}$), for the ρC nutrient addition experiments.

Experiment	1	2	3	4	5	6	
ρC	$\alpha^B_{(\text{Fe})}$ ($\times 10^{-3}$)	1.73	2.23	1.23	1.56	1.43	0.56
	$\alpha^B_{(\text{Control})}$ ($\times 10^{-3}$)	2.43	2.16	1.19	1.21	0.13	0.37
	$P_{\max}^B_{(\text{Fe})}$ ($\times 10^{-2}$)	10.67	9.30	8.46	6.22	6.04	2.86
	$P_{\max}^B_{(\text{Control})}$ ($\times 10^{-2}$)	9.23	9.14	9.48	5.99	1.06	2.56
	$E_k_{(\text{Fe})}$	61.52	41.72	68.59	39.80	42.29	51.12
	$E_k_{(\text{Control})}$	38.03	42.40	79.77	49.46	83.21	69.37

283

284 Potential drivers of variability within the photosynthetic parameters were determined through a Pearson's linear
 285 correlation coefficient matrix (Fig. 4), revealing significant negative and positive relationships with sea surface
 286 temperature (SST), salinity, nitrate and silicate concentrations, photosynthetic physiology parameters (F_v/F_m and
 287 σ_{PSII}) as well as measures of the community structure; effective diameter and ratio of Diatoms to Haptophytes.
 288 There were no significant relationships with either dissolved iron concentrations or chlorophyll concentrations.
 289 Other parameters that did not show any relationships and were excluded from the matrix include MLD, the light
 290 environment (*in situ* PAR and 1% light depth) and phosphate concentrations. α^B for the control treatments
 291 displayed the greatest number of relationships with SST, nitrate concentrations, community structure variables
 292 and F_v/F_m . The relative differences in all the parameters showed strong positive correlations with SST and
 293 salinity ($p < 0.05$). A principle component analysis (PCA) was carried out on the data with the variables' PCA
 294 projection on the factor plane represented in Fig. S3. The sum of the first two PC's explained 76.74% of the



295 total variance. The factor plane representation splits the variables, both experimental and initial conditions, into
296 the four different quadrants. The grouping of the variables within each quadrant agree with the positive
297 correlations determined within the correlation coefficient matrix; whereas variables in opposite quadrants agree
298 with the negative correlations.

299

300 3.3. Primary Production

301

302 Depth integrated primary production (PP_{wc}) was calculated at each experimental location and displayed a wide
303 range of variability with and without iron (Fig. 5). On average PP_{wc} was higher in the iron addition treatments
304 (Fig. 5a); with an average of 387.32 ± 207.18 ($\text{mg C m}^{-2} \text{d}^{-1}$) for iron addition and an average of 315.37 ± 229.37
305 ($\text{mg C m}^{-2} \text{d}^{-1}$) for the control. The maximum absolute differences in PP_{wc} (ΔPP_{wc} , Fig. 5b) of $228.82 \text{ mg C m}^{-2}$
306 s^{-1} was found in experiments 5 at $\sim 55^\circ\text{S}$ near the Southern Boundary front, with very little difference observed
307 in ΔPP_{wc} at experiments 3 and 4.

308 The responses of Fe addition to primary production from the 6 experiments were extrapolated onto
309 broader spatial and temporal scales, whereby underway measurements of Chl were converted into K_d using
310 equation 4. This, when combined with underway measurements of surface PAR allowed us to look at latitudinal
311 gradients in primary production (as per equations 1, 2 and 3). As the PE parameters displayed strong linear
312 correlations with latitude, (α $R^2 = 0.73$ and 0.66 , P_{max} $R^2 = 0.91$ and 0.68 for Fe and Control respectively), a
313 linear interpolation was applied to P_{max} and α extrapolating the values from 6 points to a 0.1° resolution along
314 the cruise track. The interpolated values of P_{max} and α were combined with underway measurements of K_d and
315 PAR to calculate PP_{wc} with and without Fe addition for the three different occupations of the same transect line
316 (Fig. 6a). A high degree of variability was revealed between occupations in the SAZ and polar frontal zone
317 (PFZ) but no clear differences between the iron and control treatments. Variability in the SAZ and PFZ appears
318 to be temporally driven, with higher values of PP_{wc} found in the third occupation of the transect line later in the
319 summer season. Differences in PP_{wc} between the two treatments become evident south of 50°S (Fig. 6a and 6b),
320 with all three iron treatment occupations being $\sim 0.5 \text{ g C m}^{-2} \text{d}^{-1}$ higher than their control treatment counterparts.
321 The differences between the control and Fe treatments were calculated for each transect, which when combined
322 allowed for the calculation of an average absolute difference in primary productivity (ΔPP_{wc} , Fig. 6c). ΔPP_{wc} is
323 slightly negative within the SAZ and PFZ, before sharply increasing to a maximum difference of $0.85 \text{ g C m}^{-2} \text{d}^{-1}$
324 at 58°S . ΔPP_{wc} begins to decrease with increasing latitude before reaching an average difference of 0.11 g C m^{-2}
325 d^{-1} in the MIZ. Representing these differences in PP_{wc} as a percentage difference (Fig. 6d) shows that within
326 the SAZ, PFZ and MIZ the differences are $\pm 10\text{-}20\%$; whereas within the Antarctic zone ($55^\circ\text{S}\text{-}65^\circ\text{S}$) the
327 differences between the treatments can be as much as 80% .

328 Given the limitations of our data set (that requires the use of interpolated values of P_{max} and α) together
329 with the weight we place on the conversion of these parameters to PP (with chlorophyll and PAR), it is
330 important that we understand the sensitivity of the PP model to variability in the different input parameters. To
331 test this, we performed a series of sensitivity tests to determine which components present the greatest influence
332 on the final PP values. The sensitivity tests were divided into the three components of the equation; K_d derived
333 from chlorophyll (Fig. S4), surface PAR (Fig. S5) and the photosynthetic parameters (P_{max} and α) (Fig. S6). For
334 consistency, the range of variation for each parameter was calculated and used as a factor to alter each



335 component. The mean range of variability for K_d was 84.33%, surface PAR was 68.73%, and α and P_{\max} were
336 82.85% and 83.01% respectively. If K_d values are increased by 84.33% this results in a 29.61% decrease in
337 ΔPP_{wc} , whereas a decrease of K_d results in an increase in ΔPP_{wc} , of 59.17%. Increasing surface PAR resulted in
338 an increase in ΔPP_{wc} of 3.50%; whilst decreasing PAR corresponded to a decrease of 8.06%. The largest
339 differences in ΔPP_{wc} were generated when P_{\max} was altered by 83.01%, in accordance with the range of
340 variability, resulting in an increase of 42.97% and a decrease of 80.92% in ΔPP_{wc} (for an increase and decrease
341 in P_{\max} respectively). The other PE parameter, α , did not result in the same level of changes in ΔPP_{wc} and only
342 increased by 4.01% and decreased by 12.22% for an increase and decrease in α by 82.85% respectively.

343 **4. Discussion**

344

345 Phytoplankton biomass in the Southern Ocean is potentially limited in their extent and magnitude
346 predominantly by the availability of the micronutrient iron (Blain et al., 2007; Boyd et al., 2000; Pollard et al.,
347 2009). This conclusion is based on the combination of two factors, the high iron requirements for photosynthetic
348 proteins (Shi et al., 2007) and the lack of supply sources of iron to the Southern Ocean (Duce and Tindale, 1991;
349 Tagliabue et al., 2014). The result of which is an environment that displays high degrees of spatial and temporal
350 variability in primary production in response to highly variable iron supply mechanisms that result in
351 chlorophyll patchiness (Fig. 1) and a complex seasonality (Thomalla et al., 2011). Iron limitation is potentially
352 strongest during the summer months when light levels are not considered limiting and the spring bloom is
353 expected to have utilised the bulk of the winter iron resupply. In the austral summer of 2015/2016 a series of
354 iron addition photosynthesis versus irradiance experiments were performed in the Atlantic Southern Ocean to
355 determine the extent to which iron availability was limiting maximal rates of primary productivity.

356 The addition of iron appeared to stimulate increased productivity to varying degrees (Fig. 2, Fig. 3b,
357 Fig. S1, Fig. S2) with average P_{\max} and α values being higher for an iron replete system (12.75 ± 6.95 and
358 0.25 ± 0.14) compared to a control system (11.17 ± 8.23 and 0.22 ± 0.19), suggestive that iron is indeed a
359 micronutrient limiting phytoplankton production in this region. Similar responses have been reported by
360 Hiscock et al. (2008) under conditions of sub-saturating light conditions, where the addition of iron can result in
361 a doubling of photosynthetic rates. However, a nutrient addition PE experiment in the Ross Sea demonstrated no
362 significant increases in α^B or P^B_{\max} (Smith and Donaldson, 2015). One potential reason for this is the length of
363 their incubation period, which was only 2 hours and may not have been sufficient enough for the phytoplankton
364 to incorporate the iron into their proteins and produce higher productivity rates. Indeed, nutrient addition
365 experiments performed under similar conditions were shown to require 24 hours to see any significant
366 differences in photophysiology (Ryan-Keogh et al., 2017; Ryan-Keogh et al., 2013) with changes in biomass
367 only being reported after 48 hours. This shortcoming highlights the attraction of the unique experimental design
368 utilised here, which allows for 24-hour Fe addition and control incubations at varying light levels and constant
369 temperature.

370 Potential factors that are known to be associated with iron-induced enhanced primary productivity
371 include temperature, macronutrient concentrations, Chl, MLD, light history and community composition. A
372 Pearson's linear correlation matrix (Fig. 4) was carried out on an array of variables to examine the influence of
373 key physical, chemical and biological factors on the variability of photosynthetic parameters in this study.
374 Significant relationships were found with SST, salinity and macronutrient concentrations, which show strong
375 latitudinal gradients. A proxy for the community structure that utilized the ratio of the 2 dominant groupings
376 (Diatoms and Haptophytes) also indicated strong significant relationships with the PE parameters. No
377 significant relationships were however found between PE parameters and iron or Chl concentrations. The lack
378 of significant relationships could be due to the small range of variability observed in these parameters; for
379 example, Chl concentrations at all stations were typically low ($0.84 - 2.30 \mu\text{g L}^{-1}$) as were dissolved iron
380 concentrations ($0.03 - 0.17 \text{ nM}$). The lack of a relationship with dissolved iron concentrations highlights how
381 this proxy is not necessarily a good indicator of iron stress, as any limiting nutrient would be expected to be



382 severely depleted by biological uptake with a resultant ambient concentration that would remain close to zero
383 despite possible event scale supply (Ryan-Keogh et al., 2017).

384 The photosynthetic parameters derived here are important components in a suite of models that derive
385 estimates of phytoplankton primary production (Behrenfeld and Falkowski, 1997a, b; Sathyendranath and Platt,
386 2007). Different primary production models inherently consist of certain biases towards modelling the
387 photosynthetic parameters whereas others have excluded them entirely from the computation of primary
388 productivity rates. Hiscock et al. (2008) demonstrated that the variables in the Behrenfeld and Falkowski
389 (1997b) standard depth-integrated model (DIM) exerted considerably different forcing mechanisms on the final
390 primary productivity rates. In the case of this DIM, phytoplankton biomass was the dominant variable that could
391 result in three orders of magnitude changes in primary production, compared to only a 40-fold change when
392 altering the photosynthetic parameter P_{opt}^B (i.e. P_{max}^B). This highlights the need to understand the sensitivity of
393 different PP models to variability within their input parameters.

394 Results from the production model applied here (equations 1, 2 and 3) show a general decrease with
395 latitude in depth-integrated primary production (PP_{wc}), with significant differences between treatments (t-test,
396 $p < 0.05$). One station near the Southern Boundary exhibited the greatest differences in ΔPP_{wc} with a value of
397 $0.89 \text{ g C m}^{-2} \text{ d}^{-1}$ (Fig. 5b), with the lowest observed ΔPP_{wc} of $0.11 \text{ g C m}^{-2} \text{ d}^{-1}$ south of the polar front. The low
398 sampling frequency of the experiments both spatially and temporally (6 experiments spanning two months and
399 the entire latitudinal extent of the Southern Ocean) together with the diverse range of initial set up conditions
400 (Table 1) make it difficult to interpret the causal relationships observed within each experiment with any
401 certainty. Instead, the information from these experiments were maximised through an alternate approach that
402 utilised the range of variability in PE parameters in control versus iron addition experiments to gain a broader
403 spatial interpretation of the response of phytoplankton production to iron addition.

404 A linear interpolation of the PE parameters (P_{max} and α) with latitude, together with underway
405 measurements of PAR and K_d (derived from surface Chl) allow for the generation of high resolution rates of
406 PP_{wc} with and without Fe addition for three occupations of the cruise transect (Fig. 6a). Within the SAZ and
407 PFZ there was a high degree of variability between the three occupations, with higher PP_{wc} values later in the
408 growing season (Fig. 6a). However, there were no clear differences between the iron and control treatments in
409 any of the occupations. Whereas south of 50°S there were no differences as the growing season progressed but a
410 clear difference between the iron and control treatments (Fig. 6b and 6c). Here, a maximum percentage
411 difference of $\sim 80\%$ (Fig. 6d) was observed between control and iron replete conditions, with ΔPP_{wc} peaking at
412 $0.85 \text{ g C m}^{-2} \text{ y}^{-1}$ at 55°S . Differences between iron addition and control systems begin to decline within the MIZ
413 (Fig. 6c). These results suggest that there are potential differences in iron availability and supply within different
414 zones of the Southern Ocean, which agrees with previous studies which postulated that the bloom extent and
415 duration within the SAZ could potentially be driven by enhanced iron supply through storm-eddy interaction
416 (Nicholson et al., 2016) while in the MIZ addition iron is supplied through melting ice (Gao et al., 2003; Grotti
417 et al., 2005; Sedwick and DiTullio, 1997). The Fe addition test performed here demonstrates the sensitivity of
418 waters south of 50°S to Fe availability, if models do not consider this sensitivity then the degree of error for PP
419 models can be as high as 80%.

420 From these results, it became clear that higher values of P_{max} and α because of iron addition were
421 significantly influencing the model outputs of primary production. However, the extent to which changes in the



422 PE parameters were responsible for the latitudinal trend in ΔPP_{wc} versus changes in ancillary parameters (e.g.
423 Chl, PAR) is unclear. To test our interpretation of the variability in PP_{wc} being a direct response to Fe
424 availability through changes in the PE parameters, a series of sensitivity analyses were performed which showed
425 that PAR and α exerted very little influence (Fig. S5 and S6). Biomass (Chl), as represented through K_d , did
426 exert a large influence on PP_{wc} (up to 59%, Fig. S4), however the greatest influence was P_{max} (up to 81%, Fig.
427 S6). As such, we can conclude that the primary driver of the latitudinal trend in ΔPP_{wc} is the result of changes in
428 the maximum photosynthetic capacity (P_{max}) to iron addition.

429 The photosynthetic parameters P_{max} and α remain difficult to fully parameterise due to interacting
430 effects of iron, light availability, temperature and community structure, yet these parameters remain critical
431 components of different biogeochemical models. Our results show that if models fail to capture the interacting
432 effects of iron and other parameters on primary productivity, then the degree of error across vast extents of the
433 Southern Ocean can be significant (as much as 80%). On the other hand, any model that can correctly account
434 for variability in these parameters will better reproduce the natural background levels of primary productivity
435 and the seasonal cycle for application to iron limited areas of the ocean including the Sub-Arctic Pacific and the
436 Southern Ocean.

437

438 **Acknowledgements**

439

440 We would like to thank the South African National Antarctic Programme (SANAP) and the captain and crew of
441 the SA Agulhas II for their professional support throughout the cruise. Ryan Cloete and Ryan Miltz were
442 involved in experimental set up; Natasha van Horsten and Warren Joubert performed the DIC determinations for
443 calculation of carbon assimilation. This work was undertaken and supported through the CSIR's Southern
444 Ocean Carbon and Climate Observatory (SOCCO) Programme (<http://socco.org.za/>). This work was supported
445 by CSIR's Parliamentary Grant funding and the NRF SANAP grant (SNA14073184298).

446 **References**

447

- 448 Arrigo, K. R., Perovich, D. K., Pickart, R. S., Brown, Z. W., van Dijken, G. L., Lowry, K. E., Mills, M. M.,
 449 Palmer, M. A., Balch, W. M., Bahr, F., Bates, N. R., Benitez-Nelson, C., Bowler, B., Brownlee, E., Ehn, J. K.,
 450 Frey, K. E., Garley, R., Laney, S. R., Lubelczyk, L., Mathis, J., Matsuoaka, A., Mitchell, B. G., Moore, G. W.
 451 K., Ortega-Retuerta, E., Pal, S., Polashenski, C. M., Reynolds, R. A., Scheiber, B., Sosik, H. M., Stephens, M.,
 452 and Swift, J. H.: Massive phytoplankton blooms under Arctic sea ice, *Science*, 336, 1408,
 453 10.1126/science.1215065, 2013.
- 454 Baker, N. R., Oxborough, K., Lawson, T., and Morrison, J. I. L.: High resolution imaging of photosynthetic
 455 activities of tissues, cells and chloroplasts in leaves, *J Exp Bot*, 52, 615-621, 10.1093/jexbot/52.356.615, 2001.
- 456 Behrenfeld, M. J. and Falkowski, P. G.: A consumer's guide to phytoplankton primary productivity models,
 457 *Limnol Oceanogr*, 42, 1479-1491, 10.4319/lo.1997.42.7.1479, 1997a.
- 458 Behrenfeld, M. J. and Falkowski, P. G.: Photosynthetic rates derived from satellite-based chlorophyll
 459 concentration, *Limnol Oceanogr*, 42, 1-20, 10.4319/lo.1997.42.1.0001, 1997b.
- 460 Blain, S., Queguiner, B., Armand, L., Belviso, S., Bombled, B., Bopp, L., Bowie, A., Brunet, C., Brussaard, C.,
 461 Carlotti, F., Christaki, U., Corbiere, A., Durand, I., Ebersbach, F., Fuda, J. L., Garcia, N., Gerringa, L., Griffiths,
 462 B., Guigue, C., Guillerm, C., Jacquet, S., Jeandel, C., Laan, P., Lefevre, D., Lo Monaco, C., Malits, A., Mosseri,
 463 J., Obernosterer, I., Park, Y. H., Picheral, M., Pondaven, P., Remenyi, T., Sandroni, V., Sarthou, G., Savoye, N.,
 464 Scouarnec, L., Souhaut, M., Thuiller, D., Timmermans, K., Trull, T., Uitz, J., van Beek, P., Veldhuis, M.,
 465 Vincent, D., Viollier, E., Vong, L., and Wagener, T.: Effect of natural iron fertilization on carbon sequestration
 466 in the Southern Ocean, *Nature*, 446, 1070-1074, 10.1038/nature05700, 2007.
- 467 Boyd, P. W., Crossely, A. C., DiTullio, G. R., Griffiths, F. B., Hutchins, D. A., Queguiner, B., Sedwick, P. N.,
 468 and Trull, T. W.: Control of phytoplankton growth by iron supply and irradiance in the subantarctic Southern
 469 Ocean: Experimental results from the SAZ Project, *J Geophys Res*, 106, 31573-31583, 10.1029/2000JC000348,
 470 2001.
- 471 Boyd, P. W. and Doney, S. C.: Modelling regional responses by marine pelagic ecosystems to global climate
 472 change, *Geophysical Research Letters*, 29, 10.1029/2001GL014130, 2002.
- 473 Boyd, P. W., Watson, A. J., Law, C. S., Abraham, E. R., Trull, T., Murdoch, R., Bakker, D. C. E., Bowie, A. R.,
 474 Buesseler, K. O., Chang, H., Charette, M., Croot, P., Downing, K., Frew, R., Gall, M., Hadfield, M., Hall, J.,
 475 Harvey, M., Jameson, G., LaRoche, J., Liddicoat, M., Ling, R., Maldonado, M. T., McKay, R. M., Nodder, S.,
 476 Pickmere, S., Pridmore, R., Rintoul, S., Safi, K., Sutton, P., Strzepek, R., Tanneberger, K., Turner, S., Waite,
 477 A., and Zeldis, J.: A mesoscale phytoplankton bloom in the polar Southern Ocean stimulated by iron
 478 fertilization, *Nature*, 407, 695-702, 10.1038/35037500, 2000.
- 479 Cochlan, W. P.: Nitrogen Uptake in the Southern Ocean. In: *Nitrogen in the Marine Environment*, Elsevier,
 480 Amsterdam, 2008.
- 481 Cullen, J. J. and Davis, R. F.: The blank can make a big difference in oceanographic measurements, *Limnology
 482 and Oceanography Bulletin*, 12, 29-35, 10.1002/lob.200312229, 2003.
- 483 de Baar, H. J. W., Boyd, P. W., Coale, K. H., Landry, M. R., Tsuda, A., Assmy, P., Bakker, D. C. E., Bozec, Y.,
 484 Barber, R. T., Brezinski, M. A., Buesseler, K. O., Boyé, M., Croot, P. L., Gervais, F., Gorbunov, M. Y.,
 485 Harrison, P. J., Hiscock, W. T., Laan, P., Lancelot, C., Law, C. S., Levasseur, M., Marchetti, A., Millero, F. J.,



- 486 Nishioka, J., Nojiri, Y., van Oijen, T., Riebesell, U., Rijkenberg, M. J. A., Saito, H., Takeda, S., Timmermans,
 487 K. R., Veldhuis, M. J. W., Waite, A. M., and Wong, C. S.: Synthesis of iron fertilization experiments: From the
 488 iron age in the age of enlightenment, *J Geophys Res*, 110, C09S16, 10.1029/2004JC002601, 2005.
- 489 de Baar, H. J. W., Buma, A. G. J., Nolting, R. F., Cadee, G. C., Jacques, G., and Treguer, P. J.: On iron
 490 limitation of the Southern Ocean: Experimental observations in the Weddell and Scotia Seas, *Mar Ecol Prog*
 491 *Ser*, 65, 105-122, 1990.
- 492 de Boyer Montégut, C., Madec, G., Fischer, A. S., Lazar, A., and Iudicone, D.: Mixed layer depth over the
 493 global ocean: an examination of profile data and a profile-based climatology, *J Geophys Res*, 109, C12003,
 494 10.1029/2004JC002378, 2004.
- 495 Dower, K. M. and Lucas, M. I.: Photosynthesis-irradiance relationships and production associated with a warm-
 496 core ring shed from the Agulhas Retroflection south of Africa, *Mar Ecol Prog Ser*, 95, 141-154,
 497 10.3354/meps095141, 1993.
- 498 Dubischar, C. D. and Bathmann, U. V.: Grazing impacts of copepods and salps on phytoplankton in the Atlantic
 499 sector of the Southern Ocean, *Deep-Sea Research II*, 44, 415-433, 10.1016/S0967-0645(96)00064-1, 1997.
- 500 Duce, R. A. and Tindale, N. W.: Atmospheric Transport of Iron and Its Deposition in the Ocean, *Limnol*
 501 *Oceanogr*, 36, 1715-1726, 10.4319/lo.1991.36.8.1715, 1991.
- 502 Dugdale, R. C. and Wilkerson, F. P.: The use of ^{15}N to measure nitrogen uptake in eutrophic oceans;
 503 experimental considerations, *Limnol Oceanogr*, 31, 673-689, 10.4319/lo.1986.31.4.0673, 1986.
- 504 Egan, L.: QuickChem Method 31-107-04-1-C - Nitrate and/or Nitrite in brackish or seawater, Lachat
 505 Instruments, 2008.
- 506 Feng, Y., Hare, C. E., Rose, J. M., Handy, S. M., DiTullio, G. R., Lee, P. A., Smith, W. O., Jr., Peloquin, J.,
 507 Tozzi, S., Sun, J., Zhang, Y., Dunbar, R. B., Long, M. C., Sohst, B., Lohan, M., and Hutchins, D. A.: Interactive
 508 effects of iron, irradiance and CO_2 on Ross Sea phytoplankton, *Deep-Sea Research I*, 57, 368-383,
 509 10.1016/j.dsr.2009.10.013, 2010.
- 510 Gao, Y., Fan, S.-M., and Sarmiento, J. L.: Aeolian iron input to the ocean through precipitation scavenging: A
 511 modeling perspective and its implication for natural iron fertilization in the ocean, *J Geophys Res*, 108,
 512 10.1029/2002JD002420, 2003.
- 513 Gibberd, M.-J., Kean, E., Barlow, R., Thomalla, S., and Lucas, M.: Phytoplankton chemotaxonomy in the
 514 Atlantic sector of the Southern Ocean during late summer 2009, *Deep-Sea Research I*, 78, 70-78,
 515 10.1016/j.dsr.2013.04.007, 2013.
- 516 Grasshoff, K., Ehrhardt, M., and Kremling, K.: Methods of seawater analysis, Verlag Chemie, Weinheim,
 517 Germany, 1983.
- 518 Grotti, M., Soggia, F., Ianni, C., and Frache, R.: Trace metals distributions in coastal sea ice of Terra Nova Bay,
 519 Ross Sea, Antarctica, *Antarct Sci*, 17, 289-300, 2005.
- 520 Hansen, J. E. and Travis, L. D.: Light scattering in planetary atmospheres, *Space Science Reviews*, 16, 527-610,
 521 10.1007/BF00168069, 1974.
- 522 Hiscock, M. R., Lance, V. P., Apprill, A. M., Johnson, Z., Bidigare, R. R., Mitchell, B. G., Smith, W. O. J., and
 523 Barber, R. T.: Photosynthetic maximum quantum yield increases are an essential component of Southern Ocean
 524 phytoplankton iron response, *Proc Natl Acad Sci U S A*, 105, 4775-4780, 10.1073/pnas.0705006105, 2008.



- 525 Hopkinson, B. M., Mitchell, B. G., Reynolds, R. A., Wang, H., Selph, K. E., Measures, C. I., Hewes, C. D.,
 526 Holm-Hansen, O., and Barbeau, K. A.: Iron limitation across chlorophyll gradients in the southern Drake
 527 Passage: Phytoplankton responses to iron addition and photosynthetic indicators of iron stress, *Limnol*
 528 *Oceanogr.*, 52, 2540-2554, 10.4319/lo.2007.52.6.2540, 2007.
- 529 Johnson, K. S., Elrod, V. A., Fitzwater, S. E., Plant, J., Boyle, E., Bergquist, B., Bruland, K. W., Aguilar-Islas,
 530 A. M., Buck, K., Lohan, M. C., Smith, G. J., Sohst, B. M., Coale, K. H., Gordon, M., Tanner, S., Measures, C.
 531 I., Moffett, J., Barbeau, K. A., King, A., Bowie, A. R., Chase, Z., Cullen, J. J., Laan, P., Landing, W., Mendez,
 532 J., Milne, A., Obata, H., Doi, T., Ossiander, L., Sarthou, G., Sedwick, P. N., Van den Berg, S., Laglera-Baquer,
 533 L., Wu, J.-F., and Cai, Y.: Developing standards for dissolved iron in seawater, *Eos, Transactions American*
 534 *Geophysical Union*, 88, 131-132, 10.1029/2007EO110003, 2007.
- 535 Khatiwala, S., Primeau, F., and Hall, T.: Reconstruction of the history of anthropogenic CO₂ concentrations in
 536 the ocean, *Nature*, 462, 346-349, 10.1038/nature08526, 2009.
- 537 Kolber, Z. S., Prášil, O., and Falkowski, P. G.: Measurements of variable chlorophyll fluorescence using fast
 538 repetition rate techniques: defining methodology and experimental protocols, *Biochim Biophys Acta*, 1367, 88-
 539 106, 10.1016/S0005-2728(98)00135-2, 1998.
- 540 Lucas, M., Seeyave, S., Sanders, R., Moore, C. M., Williamson, R., and Stinchcombe, M.: Nitrogen uptake
 541 responses to a naturally Fe-fertilised phytoplankton bloom during the 2004/2005 CROZEX study, *Deep-Sea*
 542 *Research II*, 54, 2138-2173, 10.4319/lo.2007.52.6.2540, 2007.
- 543 Mackey, M. D., Mackey, D. J., Higgins, H. W., and Wright, S. W.: CHEMTAX - a program for estimating class
 544 abundances from chemical markers: application to HPLC measurements of phytoplankton, *Mar Ecol Prog Ser*,
 545 144, 265-283, 10.3354/meps144265, 1996.
- 546 Maldonado, M. T., Boyd, P. W., Harrison, P. J., and Price, N. M.: Co-limitation of phytoplankton growth by
 547 light and Fe during winter in the NE subarctic Pacific Ocean, *Deep-Sea Research II*, 46, 2475-2485,
 548 10.1016/S0967-0645(99)00072-7, 1999.
- 549 Martin, J. H., Gordon, R. M., and Fitzwater, S. E.: Iron in Antarctic waters, *Nature*, 345, 156-158,
 550 10.1038/345156a0, 1990.
- 551 Mikaloff Fletcher, S. E., Gruber, N., Jacobson, A. R., Doney, S. C., Dutkiewicz, S., Gerber, M., Follows, M.,
 552 Joos, F., Lindsay, K., Menemenlis, D., Mouchet, A., Müller, S. A., and Sarmiento, J. L.: Inverse estimates of
 553 anthropogenic CO₂ uptake, transport, and storage by the the ocean, *Global Biogeochemical Cycles*, 20, GB2002,
 554 10.1029/2005GB002530, 2006.
- 555 Milligan, A. J. and Harrison, P. J.: Effects of non-steady-state iron limitation on nitrogen assimilatory enzymes
 556 in the marine diatom *Thalassiosira weissflogii* (Bacillariophyceae), *J Phycol*, 36, 78-86, 10.1046/j.1529-
 557 8817.2000.99013.x, 2000.
- 558 Montes-Hugo, M., Doney, S. C., Ducklow, H. W., Fraser, W., Martinson, D., Stammerjohn, S. E., and
 559 Schofield, O.: Recent changes in phytoplankton communities associated with rapid regional climate change
 560 along the Western Antarctic Peninsula, *Science*, 323, 1470-1473, 10.1126/science.1164533, 2008.
- 561 Moore, C. M., Mills, M. M., Arrigo, K. R., Berman-Frank, I., Bopp, L., Boyd, P. W., Galbraith, E. D., Geider,
 562 R. J., Guieu, C., Jaccard, S. L., Jickells, T. D., La Roche, J., Lenton, T. M., Mahowald, N. M., Marañón, E.,
 563 Marinov, I., Moore, J. K., Nakatsuka, T., Oschlies, A., Saito, M. A., Thingstad, T. F., Tsuda, A., and Ulloa, O.:



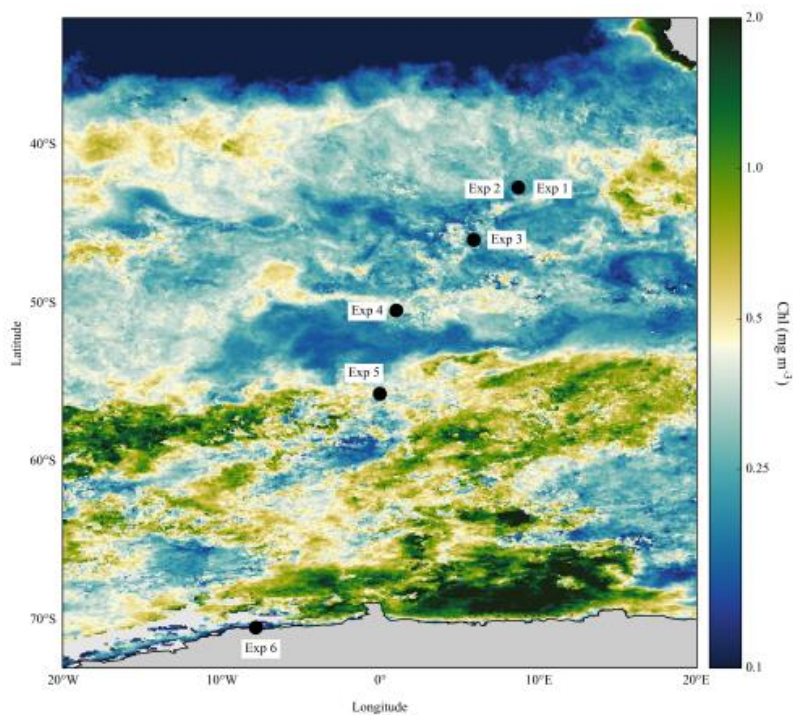
- 564 Processes and patterns of oceanic nutrient limitation, *Nature Geoscience*, 6, 701-710, 10.1038/NCEO1765,
565 2013.
- 566 Moore, C. M., Seeyave, S., Hickman, A. E., Allen, J. T., Lucas, M. I., Planquette, H., Pollard, R. T., and
567 Poulton, A. J.: Iron-light interactions during the CROZet natural iron bloom and EXport experiment (CROZEX)
568 I: Phytoplankton growth and photophysiology, *Deep-Sea Research II*, 54, 2045-2065,
569 10.1016/j.dsr2.2007.06.011, 2007.
- 570 Morel, A.: Optical modelling of the upper ocean in relation to its biogenous matter content (case 1 waters), *J*
571 *Geophys Res*, 93, 10749-10768, 10.1029/JC093iC09p10749, 1988.
- 572 Morel, A., Huot, Y., Gentili, B., Werdell, P. J., Hooker, S. B., and Franz, B. A.: Examining the consistency of
573 products derived from various ocean color sensors in open ocean (Case 1) waters in the perspective of a multi-
574 sensor approach, *Remote Sens Environ*, 111, 69-88, 10.1016/j.rse.2007.03.012, 2007.
- 575 Nicholson, S.-A., Lévy, M., Lloret, J., Swart, S., and Monteiro, P. M. S.: Investigating into the impact of storms
576 on sustaining summer primary productivity in the Sub-Antarctic Ocean, *Geophysical Research Letters*, 43,
577 10.1002/2016GL069973, 2016.
- 578 Nowlin, W. D. and Klinck, J. M.: The physics of the Antarctic Circumpolar Current, *Reviews of Geophysics*,
579 24, 469-491, 10.1029/RG024i003p00469, 1986.
- 580 Obata, H., Karatani, H., and Nakayama, E.: Automated determination of iron in seawater by chelating resin
581 concentration and chemiluminescence detection, *Anal Chem*, 65, 1524-1528, 10.1021/ac00059a007, 1993.
- 582 Orsi, A. H., Whitworth III, T. W., and Nowlin, W. D.: On the meridional extent and front of the Antarctic
583 Circumpolar Current, *Deep-Sea Research I*, 42, 641-673, 10.1016/0967-0637(95)00021-W, 1995.
- 584 Pakhomov, E. A. and Froneman, P. W.: Zooplankton dynamics in the eastern Atlantic sector of the Southern
585 Ocean during austral summer 1997/1998, *Deep-Sea Research II*, 51, 2599-2616, 10.1016/j.dsr2.2000.11.001,
586 2004.
- 587 Platt, T., Gallegos, C. L., and Harrison, W. G.: Photoinhibition of photosynthesis in natural assemblages of
588 marine phytoplankton, *Journal of Marine Research*, 38, 687-701, 1980.
- 589 Platt, T. and Sathyendranath, S.: Estimators of primary production for interpretation of remotely-sensed data on
590 ocean colour, *J Geophys Res*, 98, 14561-14576, 10.1029/93JC01001, 1993.
- 591 Platt, T., Sathyendranath, S., and Fuentes-Yaco, C.: Biological oceanography and fisheries management:
592 perspective after 10 years, *ICES J Mar Sci*, 64, 863-869, 10.1093/icesjms/fsm072, 2007.
- 593 Pollard, R. T., Salter, I., Sanders, R. J., Lucas, M. I., Moore, C. M., Mills, R. A., Statham, P. J., Allen, J. T.,
594 Baker, A. R., Bakker, D. C. E., Charette, M. A., Fielding, S., Fones, G. R., French, M., Hickman, A. E.,
595 Holland, R. J., Hughes, J. A., Jickells, T. D., Lampitt, R. S., Morris, P. J., Nedelec, F. H., Nielsdottir, M.,
596 Planquette, H., Popova, E. E., Poulton, A. J., Read, J. F., Seeyave, S., Smith, T., Stinchcombe, M., Taylor, S.,
597 Thomalla, S., Venables, H. J., Williamson, R., and Zubkov, M. V.: Southern Ocean deep-water carbon export
598 enhanced by natural iron fertilization, *Nature*, 457, 577-U581, 10.1038/nature07716, 2009.
- 599 Price, N. M., Ahner, B. A., and Morel, F. M. M.: The equatorial Pacific Ocean: Grazer-controlled phytoplankton
600 populations in an iron-limited ecosystem, *Limnol Oceanogr*, 39, 520-534, 10.4319/lo.1994.39.3.0520, 1994.
- 601 Ras, J., Claustre, H., and Uitz, J.: Spatial variability of phytoplankton pigment distributions in the Subtropical
602 South Pacific Ocean: comparison between in situ and predicted data, *Biogeosciences*, 5, 353-369, 10.5194/bg-5-
603 353-2008, 2008.



- 604 Raven, J. A.: Predictions of Mn and Fe use efficiencies of phototrophic growth as a function of light availability
 605 for growth and C assimilation pathway, *New Phytol*, 116, 1-18, 10.1111/j.1469-8137.1990.tb00505.x, 1990.
- 606 Rio, M. H., Guinehut, S., and Larnicol, G.: New CNES-CLS09 global mean dynamic topography computed
 607 from the combination of GRACE data, altimetry, and in situ measurements, *J Geophys Res*, 116, C07018,
 608 10.1029/2010JC006505, 2011.
- 609 Roháček, K.: Chlorophyll Fluorescence Parameters: The Definitions, Photosynthetic Meaning, and Mutual
 610 Relationships, *Photosynthetica*, 40, 13-29, 10.1023/A:1020125719386, 2002.
- 611 Ryan-Keogh, T. J., DeLizo, L. M., Smith, W. O., Jr., Sedwick, P. N., McGillicuddy, D. J., Jr., Moore, C. M.,
 612 and Bibby, T. S.: Temporal progression of photosynthetic strategy by phytoplankton in the Ross Sea,
 613 Antarctica, *Journal of Marine Systems*, 166, 87-96, 10.1016/j.jmarsys.2016.08.014, 2017.
- 614 Ryan-Keogh, T. J., Macey, A. I., Nielsdóttir, M., Lucas, M. I., Steigenberger, S. S., Stinchcombe, M. C.,
 615 Achterberg, E. P., Bibby, T. S., and Moore, C. M.: Spatial and temporal development of phytoplankton iron
 616 stress in relation to bloom dynamics in the high-latitude North Atlantic Ocean, *Limnol Oceanogr*, 58, 533-545,
 617 10.4319/lo.2013.58.2.0533, 2013.
- 618 Sathyendranath, S. and Platt, T.: Spectral effects in bio-optical control on the ocean system, *Oceanologia*, 49, 5-
 619 39, 2007.
- 620 Schlitzer, R.: Carbon export fluxes in the Southern Ocean: results from inverse modeling and comparison with
 621 satellite-based estimates, *Deep-Sea Research II*, 49, 1623-1644, 10.4319/lo.1994.39.3.0520, 2002.
- 622 Sedwick, P. N. and DiTullio, G. R.: Regulation of algal blooms in Antarctic shelf waters by the release of iron
 623 from melting sea ice, *Geophysical Research Letters*, 24, 2515-2518, 10.1029/97GL02596, 1997.
- 624 Shi, T., Sun, Y., and Falkowski, P. G.: Effects of iron limitation on the expression of metabolic genes in the
 625 marine cyanobacterium *Trichodesmium erythraeum* IMS101, *Environmental Microbiology*, 9, 2945-2956,
 626 10.1111/j.1462-2920.2007.01406.x, 2007.
- 627 Smetacek, V., Assmy, P., and Henjes, J.: The role of grazing in structuring Southern Ocean pelagic ecosystems
 628 and biogeochemical cycles, *Antarct Sci*, 16, 541-558, 10.1017/S0954102004002317, 2004.
- 629 Smith, W. O. J. and Donaldson, K.: Photosynthesis-irradiance responses in the Ross Sea, Antarctica: a meta-
 630 analysis, *Biogeosciences*, 12, 3567-3577, 10.5194/bg-12-3567-2015, 2015.
- 631 Strzepek, R. F. and Harrison, P. J.: Photosynthetic architecture differs in coastal and oceanic diatoms, *Nature*,
 632 431, 689-692, 10.1038/nature02954, 2004.
- 633 Strzepek, R. F., Hunter, K. A., Frew, R. D., Harrison, P. J., and Boyd, P. W.: Iron-light interactions differ in
 634 Southern Ocean phytoplankton, *Limnol Oceanogr*, 57, 1182-1200, 10.4319/lo.2012.57.4.1182, 2012.
- 635 Sunda, W. G. and Huntsman, S. A.: Interrelated influence of iron, light and cell size on marine phytoplankton
 636 growth, *Nature*, 390, 389-392, 10.1038/37093, 1997.
- 637 Swart, S., Chang, N., Fauchereau, N., Joubert, W., Lucas, M., Mtshali, T., Roychoudhury, A., Tagliabue, A.,
 638 Thomalla, S., Waldron, H., and Monteiro, P. M. S.: Southern Ocean Seasonal Cycle Experiment 2012: Seasonal
 639 scale climate and carbon cycle links, *S Afr J Sci*, 108, 11-13, 10.4102/sajs.v108i3/4.1089, 2012.
- 640 Swart, S., Speich, S., Anson, I. J., and Lutjeharms, J. R. E.: An altimetry-based gravest empirical mode south
 641 of Africa: 1. Development and validation, *J Geophys Res*, 115, C03002, 10.1029/2009JC005299, 2010.



- 642 Swart, S., Thomalla, S. J., and Monteiro, P. M. S.: The seasonal cycle of mixed layer dynamics and
643 phytoplankton biomass in the Sub-Antarctic Zone: A high-resolution glider experiment, *Journal of Marine*
644 *Systems*, 147, 103-115, 10.1016/j.jmarsys.2014.06.002, 2015.
- 645 Tagliabue, A., Sallée, J.-B., Bowie, A. R., Lévy, M., Swart, S., and Boyd, P. W.: Surface-water iron supplies in
646 the Southern Ocean sustained by deep winter mixing, *Nature Geoscience*, 7, 314-320, 10.1038/ngeo2101, 2014.
- 647 Thomalla, S. J., Fauchereau, N., Swart, S., and Monteiro, P. M. S.: Regional scale characteristics of the seasonal
648 cycle of chlorophyll in the Southern Ocean, *Biogeosciences*, 8, 2849-2866, 10.5194/bg-8-2849-2011, 2011.
- 649 Thomalla, S. J., Racault, M.-F., Swart, S., and Monteiro, P. M. S.: High-resolution view of the spring bloom
650 initiation and net community production in the Subantarctic Southern Ocean using glider data, *ICES J Mar Sci*,
651 72, 1999-2020, 10.1093/icesjms/fsv105, 2015.
- 652 Welschmeyer, N. A.: Fluorometric analysis of chlorophyll-*a* in the presence of chlorophyll-b and pheopigments,
653 *Limnol Oceanogr*, 39, 1985-1992, 10.4319/lo.1994.39.8.1985, 1994.
- 654 Wolters, M.: Quickchem Method 31-114-27-1-D - Silicate in Brackish or Seawater, Lachat Instruments, 2002.
655



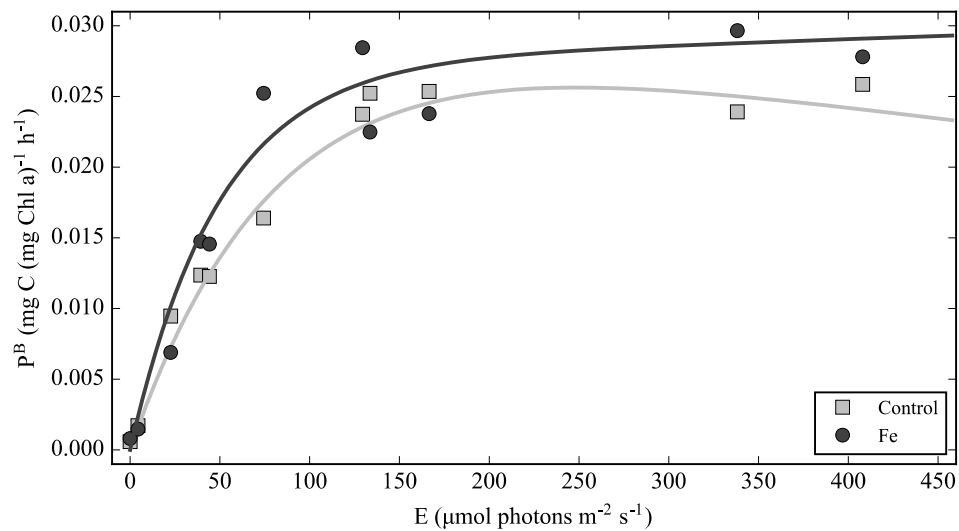
656

657 **Figure 1: Composite map of MODIS (8-day, 9 km) derived chlorophyll (mg m^{-3}) from November 2015 to March 2016**
658 **for the Atlantic sector of the Southern Ocean with locations of the nutrient addition productivity versus irradiance**
659 **(PE) experiments.**

660



661



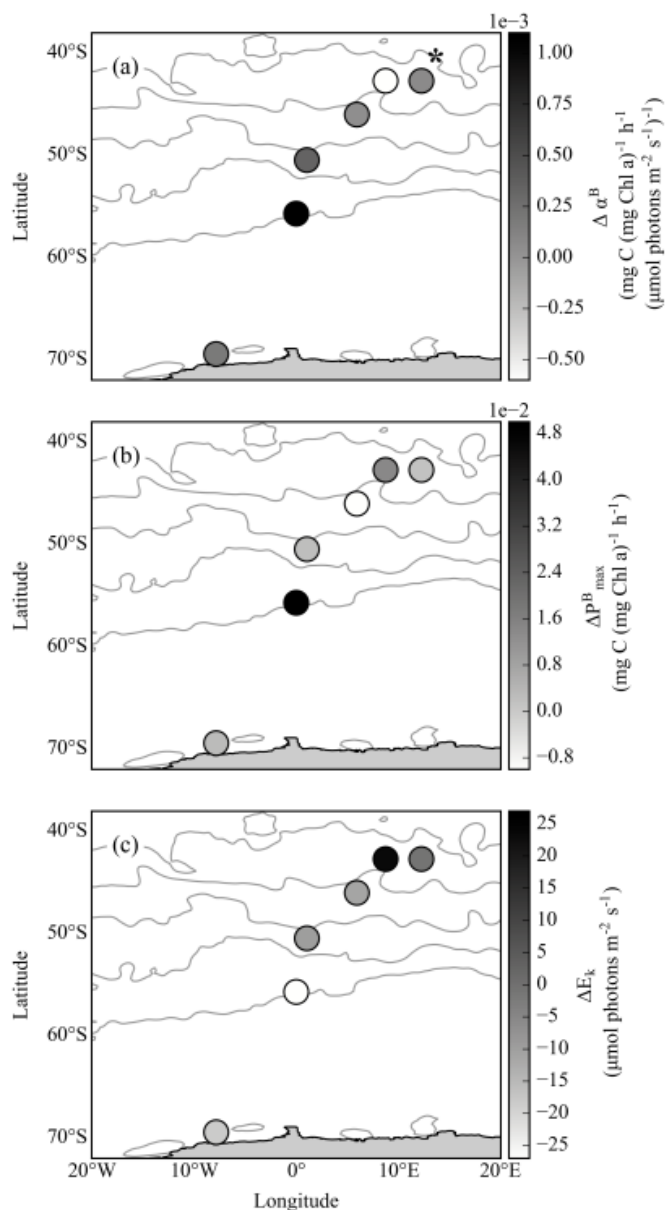
662

663 **Figure 2: An example of a PE curve of productivity (mg C (mg Chl a)⁻¹ h⁻¹), versus irradiance (μmol photons m⁻² s⁻¹),**
 664 **with (Fe) and without (Control) the addition of iron; the lines represent a non-linear least squares fit to the equation**
 665 **of Platt et al. (1980).**

666



667



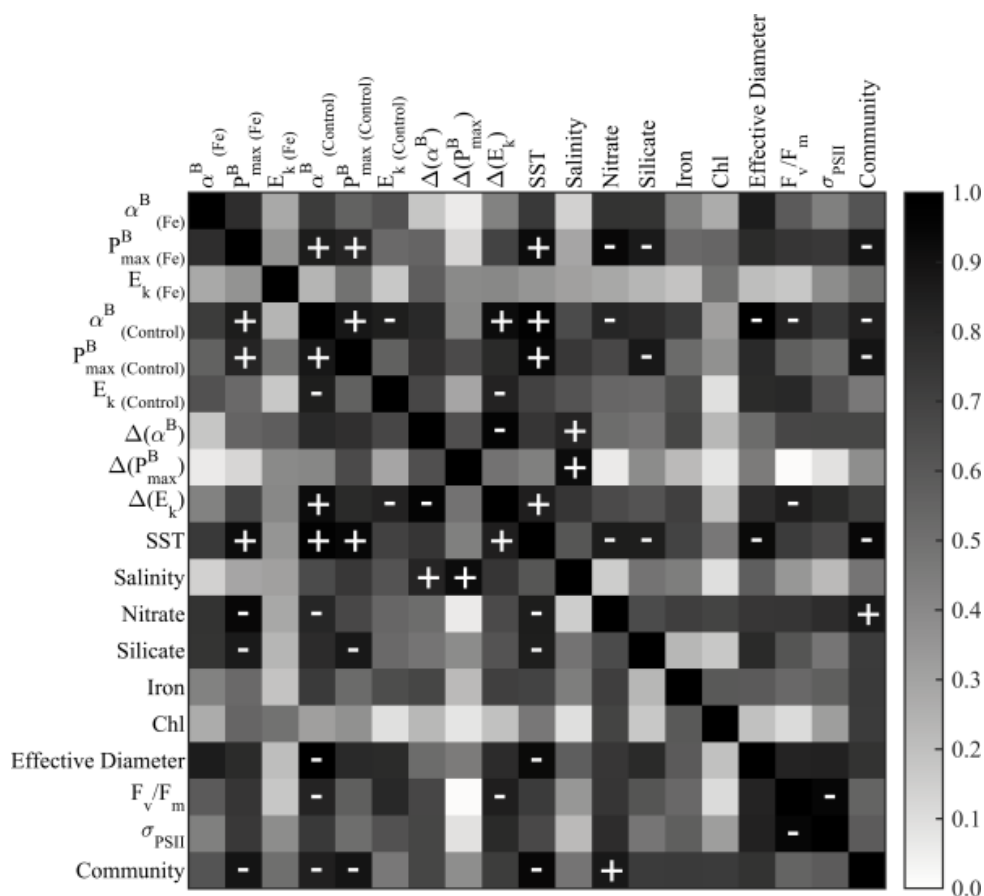
668

669 Figure 3: Experimental values of (a) $\Delta\alpha^B$ ($\text{mg C (mg Chl a)}^{-1} \text{h}^{-1}$) ($\mu\text{mol photons m}^{-2} \text{s}^{-1}$), (b) ΔP^B_{max} ($\text{mg C (mg Chl a)}^{-1} \text{h}^{-1}$) and (c) ΔE_k ($\mu\text{mol photons m}^{-2} \text{s}^{-1}$) for experiments set up in the Atlantic sector of the Southern Ocean. Ocean
 670 fronts, indicated by grey lines, were determined from MADT from the CLS/AVISO product (Rio et al., 2011) and
 671 their position averaged over 5 months (November 2015 to March 2016). From north – south: Sub-Tropical Front
 672 (STF), Sub-Antarctic Front (SAF), Antarctic Polar Front (APF), Southern Antarctic Circumpolar Front (SACCf)
 673 and the Southern Boundary (SBdy). *Position of experiment 3 moved 2.5° eastwards for presentation purposes.
 674

675



676



677

678

679

680

681

682

683

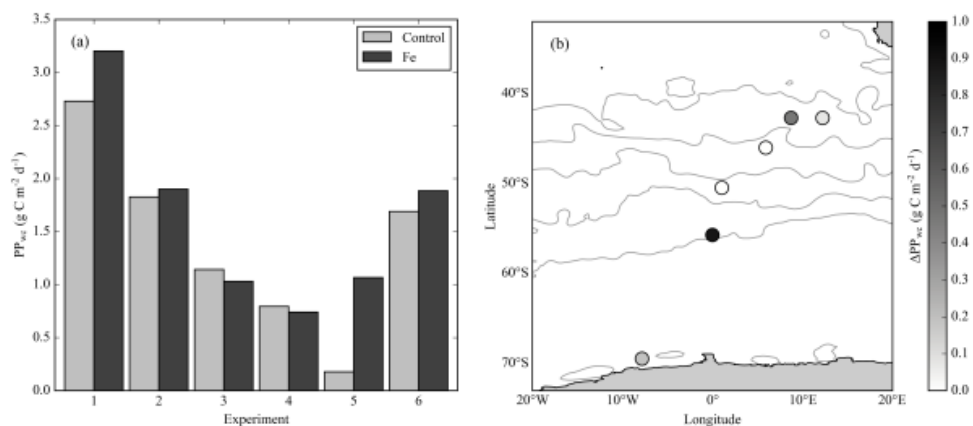
684

685

Figure 4: Matrix of Pearson's linear correlation coefficients between the photosynthetic parameters determined experimentally and *in situ* variables measured, including: α^B , P_{\max}^B and E_k from the both Fe and control treatments, the relative differences, sea surface temperature (SST), Salinity, Nitrate, Silicate and dissolved Iron concentration, Chl concentration, Effective Diameter, F_v/F_m , σ_{PSII} and Community composition (ratio of Diatoms to Haptophytes). The strength of the linear relationship associated between each pair of variables is indicated by the colour of the square, with the negative and positive correlations denoted by '-' and '+' within all squares where significant ($p < 0.05$).



686 Figure 5
687

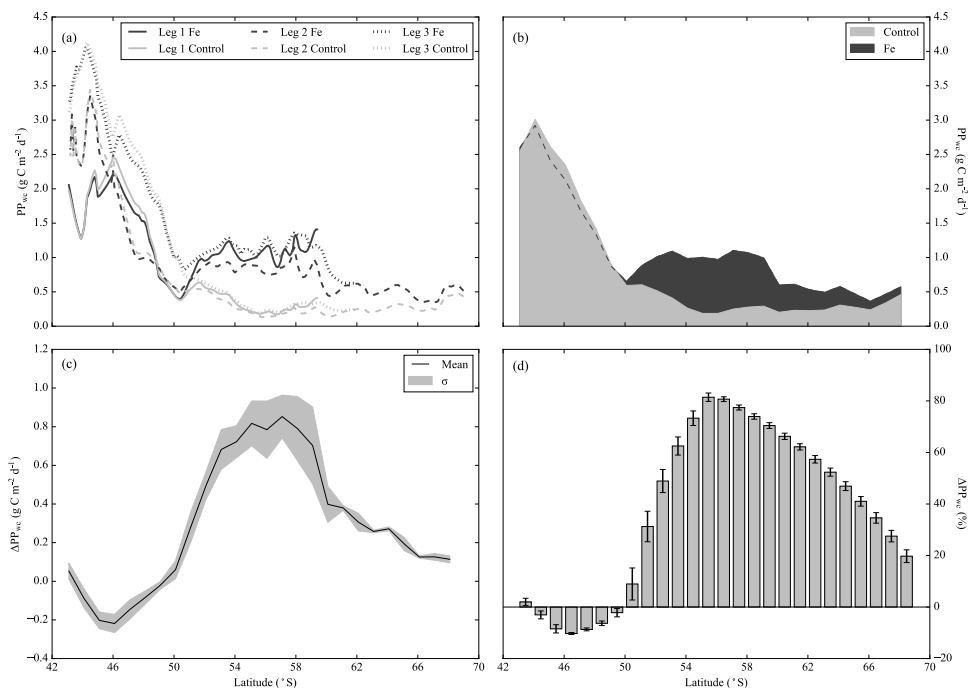


688
689
690
691
692

Figure 5: Modelled outputs of primary production utilizing experimentally derived photosynthetic parameters. (a) Depth integrated primary production (PP_{wc}) ($mg\ C\ m^{-2}\ d^{-1}$) and (b) ΔPP_{wc} ($mg\ C\ m^{-2}\ d^{-1}$). Ocean fronts, indicated by grey lines, displayed as in Fig. 3.



693



694

695 **Figure 6: Depth integrated primary production (PP_w) ($\text{mg C m}^{-2} \text{d}^{-1}$) for each transect (Leg 1 -3) (a) interpolated**
 696 **along the transect line utilizing linearly interpolated values for α and P_{max} as determined from the Fe and Control**
 697 **treatments. (b) Mean PP_w ($\text{mg C m}^{-2} \text{d}^{-1}$) with \pm standard deviation (σ). (c) The mean absolute differences in PP_w**
 698 **(ΔPP_w) with \pm standard deviation between the Fe and Control treatments. (d) ΔPP_w represented as the mean**
 699 **percentage difference with \pm standard deviations.**

700